

01

# An investigation of reading thermal images processes by a thermal image receiver made in the image intensifier tube architecture

© A.S. Grevcev, P.A. Zolotukhin, E.A. Il'ichev, G.N. Petrukhin, A.V. Popov, G.S. Rychkov

National Research University of Electronic Technology (MIET), Zelenograd, Russia  
 e-mail: edil44@mail.ru, alexcoretex@gmail.com

Received December 30, 2021

Revised February 26, 2022

Accepted February 26, 2022.

The results of calculations of electric fields, potentials, and trajectories of photoelectrons calculations of single-channel dual-spectral thermal imager, implemented in the IIT architecture are presented. The values of the optimal potentials on the control electrodes (microchannel plate, reading electrode, and photocathode) that form a picture of the images of objects and ensure the correct reading of the potential relief from the surface of the sensor-converter pyroelectric film of the image thermal receiver under discussion are determined.

**Keywords:** image intensifier tube, spontaneous polarization, a pyroelectric sensor, photocathode, photoelectronic emission, thermal object image receiver, secondary electron emission.

DOI: 10.21883/TP.2022.05.53669.338-21

## Introduction

The relevance of developing functionally efficient and cost-effective uncooled image detectors for thermal objects in relation to the image of the surrounding area is beyond dispute [1–3]. The schematic view of the studied design of an innovative single-channel thermal image receiver, made in the image intensifier tube (IIT) architecture, is shown in Fig. 1.

The mentioned detector performs functional integration of a sequence of physical effects and procedures. It includes:

- formation of images of a thermal object and the surrounding area images carried out by a single optical system in the planes of the pyroelectric sensor and photocathode locations respectively;

- conversion of an IR (0.8–1.55 μm) image of the surrounding area into an image in a photoelectron stream by means of the photoelectronic effect;

- conversion of a thermal image (3–13 μm) into a distribution pattern of pyroelectric surface potentials by means of the pyroelectric effect;

- reading by a photoelectron stream carrying information on the area surrounding the thermal object the distribution pattern of surface pyroelectric potentials induced by the image of the object thermal field;

- the multiplication of the electron stream carrying information on the thermal object and its surrounding area through the use of the effect of secondary electron emission effect;

- the transformation of the complete picture of images in the electron flux into the image of the visible part of the optical band using the cathode-ray luminescence effect.

The formation of a superposition of images of a thermal object and the surrounding area is carried out by a single optical system. The radiation of a thermal object (3–13 μm) is absorbed by a pyroelectric sensor film located in the focal plane of the thermal spectrum optical system. According to the illumination, the changes of polarization magnitude are induced, in which a distribution pattern of pyroelectric potentials is formed near the sensor surface. The surrounding area image of the thermal object (0.8–1.55 μm) is formed by reflected radiation of the night sky and is projected into the plane of the photocathode then is absorbed by its substance which causes the photoelectronic emission. Space diversity of the focal planes of a thermal object and the surrounding area images, is provided by the difference of the refraction indices of the substance of the lenses of the input optics in relation to the spectral ranges of the detected radiation. In particular, the formation of optical fluxes carrying information about a thermal object (3–13 μm) and

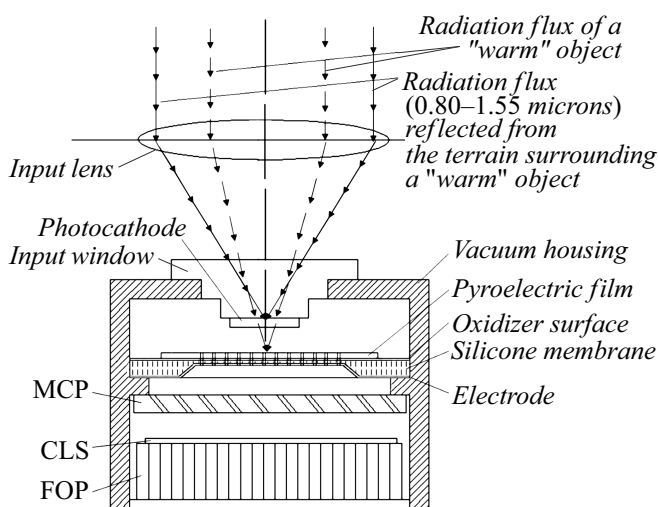


**Figure 1.** Schematic view of the design of the image detector for thermal objects, made in the architecture of the EOII.

the surrounding area (0.8–1.55  $\mu\text{m}$ ) is carried out by an optical system based on  $\text{CaF}_2$ , which allows to separate their focal planes a distance convenient for the device implementation  $\sim 1$  mm. A germanium photocathode for detecting a thermal images of a surrounding area is proposed, where the source of radiation is a reflected radiation of the night sky in the spectral range 0.8–1.55  $\mu\text{m}$ . This photocathode has an extremely high degree of transparency in the spectral range 3–15  $\mu\text{m}$ , which equal about 40% in the case of high-purity germanium and about 85% for surface coated silicon-carbon film of nanoscale thickness. A thermal object image projected through a germanium photocathode onto a pyroelectric sensor film induces on its surface a distribution pattern of potentials proportional to the magnitude of a heat flux. Information about the thermal object is integrated in the surface potential distribution of the thermal image sensor and is read by a photoelectron stream, which is additionally carrying information about a surrounding area. After interacting with the potential distribution on the surface of the thermal sensor, the photoelectron stream integrated the information of both the thermal object and the surrounding area. This stream is read through of the microchannel plate (MCP) in the direction through coaxial holes in the pyroelectric film and in the supporting silicon membrane. The resulting electron stream is amplified by the MCP by means of secondary emission effect, then it accelerated in the MCP-cathodoluminescent screen (CLS) vacuum gap and is projected onto the CLS. In CLS, images in electron stream are proportionally converted into optical images of the visible band, they are carrying information about both the thermal object and the surrounding area. The resultant image is output from the device case by means of a fiber optic plate (FOP) and then can be read visually or digital format by the CCD sensor. Between the FOP and the output window, the FOP by the immersion medium is connected. The effectiveness of under discussion the innovative thermal imager will be determined by the quality of integration of the listed physical effects and procedures.

The discussed design of the thermal imager not only binds the image of the thermal object to the image of the surrounding area, but also provides an internal gain of the electron flux, which allows to count on an acceptable threshold sensitivity of the device. The gain level is determined by the substance and design features of the MCP.

## 1. Model representations and calculation results

To optimize the design of the proposed thermal image receiver, the problem of matching the potentials of the sensory pyroelectric film and the energies of the photoelectrons of the readout beam was solved. In the computation process, the widely used equations and physical effects described below were used.

To calculate the heating dynamics of the sensor-converting film, the heat balance equation was used

$$\rho C_\rho \frac{dT}{dt} + \nabla \cdot (\mathbf{q} + \mathbf{q}_r) = \gamma P, \quad (1)$$

where  $\mathbf{q}$  — conductive heat flux

$$\mathbf{q} = -G\nabla T. \quad (2)$$

$G$  — heat conductivity factor of the multilayer structure,  $\rho$  — density,  $C_\rho$  — thermal conductivity,  $\mathbf{q}_r$  — radiative heat flux.

The heat power flux losses due to radiation ( $\mathbf{q}_r$ ) were estimated in the Stefan–Boltzmann approximation

$$\mathbf{q}_r \cdot \mathbf{n} = \gamma \sigma (T^4 - T_{initial}^4), \quad (3)$$

where  $\mathbf{n}$  — unit normal vector to the surface of the structure under study,  $T_{initial}$  — initial temperature,  $T$  — current temperature of the sensor film;  $\sigma$  — Stefan–Boltzmann constant and  $\gamma$  — emissivity factor of the sensor film surface.

Equations (1) and (4) were used to calculate the change in polarization induced by the heating of the pyroelectric film:

$$\Delta P_S = p\Delta T = p(T_{initial} - T(t)), \quad (4)$$

where  $T_{initial}$  — initial temperature,  $p$  — pyroelectric coefficient,  $\Delta P_S$  — changes of spontaneous polarization vector.

Using the equation (5) obtained by us in [5], we calculated the coordinate dependence of the electric potential on the induced polarization of the pyroelectric film at any time interval:

$$\Delta\phi(z) = \frac{\Delta P_S}{2\epsilon_0} \left( \sqrt{(z+d)^2 + R^2} - \sqrt{z^2 + R^2} - d \right). \quad (5)$$

Equation (6) was used, which describes the relationship between electric field and potential.

$$\mathbf{E} = -\nabla\phi, \quad (6)$$

where the effective electric field was obtained as a superposition of electric fields from the potentials on the photocathode, pyroelectric film, silicon membrane, and the input electrode of the MCP and the superposition of the electric fields of the photoelectron stream between themselves, associated with the Coulomb interaction (7):

$$\mathbf{E} = \mathbf{E}_{\text{PhC}} + \mathbf{E}_{\text{PF}} + \mathbf{E}_{\text{Si}} + \mathbf{E}_{\text{Coulomb}}. \quad (7)$$

Here  $\mathbf{E}_{\text{PhC}}$  — electric field intensity from photocathode potential,  $\mathbf{E}_{\text{PF}}$  — electric field intensity from potentials of the pyroelectric film,  $\mathbf{E}_{\text{Si}}$  — electric field intensity from the potential of the silicon membrane,  $\mathbf{E}_{\text{MCP}}$  — electric field intensity from the potential of the MCP input electrode,  $\mathbf{E}_{\text{Coulomb}}$  — electric field intensity associated with the

Coulomb interaction of electrons with one another, which is described by expression (8).

$$\mathbf{E}_{\text{Coul}} = \frac{1}{2} \sum_{i,j} \mathbf{E}_{ij} = \frac{1}{2} \frac{1}{q} \sum_{i,j} k \frac{q_i q_j}{r_{ij}^3} \mathbf{r}_{ij}, \quad (8)$$

where  $\mathbf{E}_{ij}$  — electric field intensity between  $i$ -th and  $j$ -th electron,  $q_i$  and  $q_j$  — charge of  $i$ -th electron,  $k$  — Coulomb coefficient,  $r_{ij}$  — radius vector between  $i$ -th and  $j$ -th electron,  $q$  — elementary electron charge, summation occurs for each  $i$ -th and  $j$ -th element, while  $i \neq j$  and  $\mathbf{E}_{ij} = \mathbf{E}_{ji}$ .

To describe the refraction of electric fields at the interface of two media with dielectric capacity  $\epsilon_1$  and  $\epsilon_2$ , equation (9) was used:

$$\frac{\text{tg } \alpha_1}{\text{tg } \alpha_2} = \frac{\epsilon_1}{\epsilon_2}, \quad (9)$$

where  $\alpha_1$  and  $\alpha_2$  — are the angles between the plane normal of the interface of two media and the electric-field vector located in the medium with dielectric capacity  $\epsilon_1$  and  $\epsilon_2$  respectively.

To describe the influence of the electric field on the photoelectron stream trajectory, equation (10) is used:

$$q\mathbf{E} = m_e \frac{dv}{dt}, \quad (10)$$

where  $q$  — elementary charge,  $m_e$  — electron mass and  $v$  — electron velocity.

When calculating the multiplication factor of the electron flux in the MCP, expression (11) was used, which represents an estimate of the number of produced secondary electrons during the interaction of electrons with the substance of the MCP:

$$n_{\text{secondary}} = \frac{E_{\text{primary}}}{E_{\text{pair form}}}, \quad (11)$$

where  $E_{\text{primary}}$  — the energy „of the primary“ electron in each cycle of interactions in the MCP channel,  $E_{\text{pair form}}$  — the energy of formation of a non-equilibrium pair of electrons–holes.

When the energy loss calculation related to convert the image in the electron flux into the optical image in the visible spectral range, the Bethe equation [4] was used.

The integration of the sequence of the listed physical effects and procedures allows to form model of image transformations and reads in a single-channel dual-spectrum thermal imager.

In the numerical model, we used the values of the induced pyroelectric potentials by thermal field, which were previously calculated and presented in the papers [5].

In this paper, the emphasis is on the theoretical analysis and numerical calculations of control potentials, which allow implementing the process of correctly reading information from the electrical potential distribution on the pyroelectric film surface. The calculations were carried out using the COMSOL Multiphysics software package (Fig. 2). The

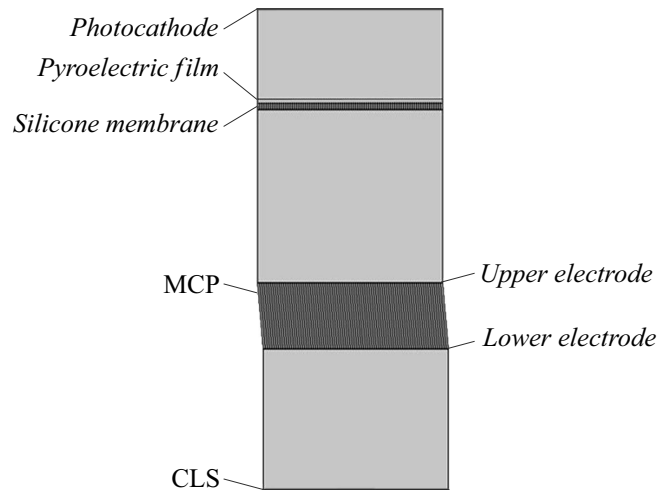


**Figure 2.** Schematic view of the reading node of a thermal imaging detector, numerically studied in the COMSOL Multiphysics software package.

object of study and analysis was an image detector consisting of the following basic units: a photocathode (based on germanium,  $0.8\text{--}1.55\ \mu\text{m}$ ); pyroelectric film ( $3\text{--}13\ \mu\text{m}$ ) located on the oxidized surface of the silicon membrane (possible —  $\text{SiO}_2/\text{Me}/\text{MCP}$ ); microchannel plate (MCP); cathodoluminescent screen (CLS).

Preliminary estimates and results of experimental studies [5] were used in this paper as the initial values of the pyroelectric potential and the initial energy of the electron reading stream, which amounted to  $-1\ \text{V}$  and  $0.5\ \text{eV}$ , respectively.

### 1.1. Investigations and search of silicon membrane potential

The silicon membrane was used as a readout electrode, which provides greater flexibility in shaping and controlling the readout electron stream path. The variation of the potential of the silicon membrane allows improving the reading process of information from the pyroelectric sensor by the photoelectron stream. The optimal parameters of control potentials of silicon membrane are calculated, which reduce the probability of information distortion due to the capture of photoelectrons by the pyroelectric film. The calculations results are presented in Fig. 3.

The time dependence characteristics of the captured photoelectrons number on the Si membrane potential were analyzed, while a potential equal to  $-1\ \text{V}$  was applied to the photocathode, and a potential of  $30\ \text{V}$  was applied to the upper MCP electrode. An array of a hundred (100) photoelectrons emitted by a photocathode, and they are carrying information on the intensity of radiation reflected from the surrounding area ( $0.8\text{--}1.55\ \mu\text{m}$ ) was used as a readout electron stream in the simulation.

Using the time dependence of the number of captured photoelectrons by the pyroelectric film (Fig. 3), the numbers

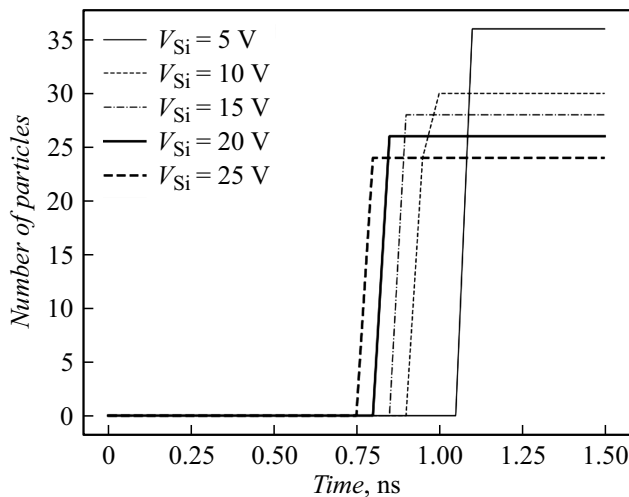


**Figure 3.** Time dependence of the number of photoelectrons captured by the pyroelectric film on the potential of the silicon membrane.

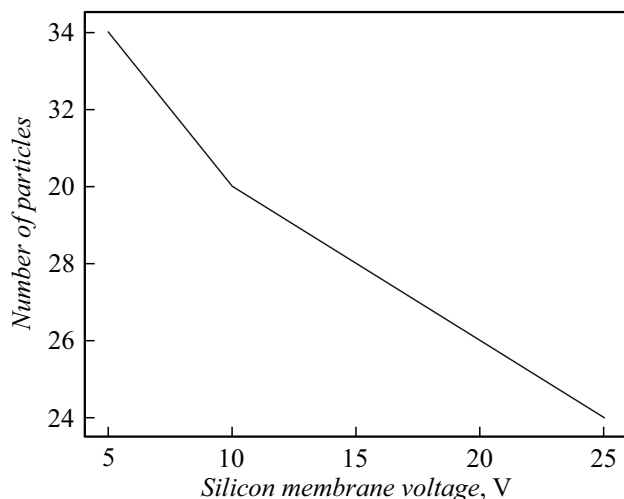


**Figure 4.** Dependence of the number of photoelectrons captured by the pyroelectric film in the stationary area on the potential of the silicon membrane.

of captured electrons in the plateau region were obtained, which were used to plotted figure (Fig. 4).

Fig. 4 illustrates the monotonic decreasing of the maximum photoelectrons number of readout electron stream captured by the pyroelectric sensor with increasing in the potential value at the readout electrode of a silicon membrane.

To identify parasitic effects of information reading about a thermal object related to the value of the potential of the silicon membrane, the photoelectrons paths in the space between the silicon membrane and the MCP input electrode were calculated. The results are shown in Figures 5 and 6 at silicon membrane potentials of 5 V and 25 V, respectively. Meanwhile, the potential of the input electrode of the MCP was fixed at a level of 30 V.

The analysis of the readout electron stream path at different potentials on the silicon membrane showed that an excessive increase in the potential of the silicon membrane leads to defocusing of the electronic distribution of the thermal image (Fig. 5, *b*). Therefore, when searching for the optimal value of the potential of the silicon membrane, it is required to maintain a balance between the number of electrons captured by the pyroelectric film and the degree of defocusing of the electron stream. According to the results of calculations, the optimal value of the control potential on the silicon membrane lies in the range of 10–15 V, and the problem of the mentioned distortions can be additionally corrected by increasing the potential at the MCP input electrode.

## 1.2. Investigations and search of MCP electrodes potential

When selecting potentials on the MCP electrodes, it is also required to take into account the opportunity of performance of various (including parasitic) influence factors. Obviously, the potential difference between the input and output electrodes determines the multiplication factor of the electron stream, which is limited by the electrical intensity limit of the MCP substance, and is shown in Fig. 7. The number of multiplied electrons grows exponentially with an increase in the potential difference between the input and output electrodes of the MCP.

It is also obvious that the potential at the MCP input electrode should be significantly exceeded by the ratio  $E_{pair\ form}/q$ , where  $E_{pair\ form}$  — energy of formation of secondary electrons,  $q$  — elementary charge. On the Fig. 8 the saturation of the number of multiplied electrons is observed, when the potential difference of 500 V is fixed and the top electrode of the MCP voltage equal about 80–100 V.

The potential value influences of the MCP input electrode on the degree of defocusing of the total image of thermal object and surrounding area integrated in the electron stream is less obvious. To assess the influence of the potential of the input MCP electrode on the reading thermal image process, the electron stream trajectory between the silicon membrane and the MCP (Fig. 6) is calculated and plotted. Meanwhile, the potential on the silicon membrane was fixed at the level of 10 V, and the potential on the photocathode was chosen equal to  $-1$  V, the potential difference between the MCP electrodes was  $\sim 500$  V. The potential at the output MCP electrode was chosen equal to  $\sim 600$  V.

From Fig. 6 it follows that the degree of defocusing of electronic stream is minimized, when the potential at the input electrode of the MCP value increases up to 100V. Meanwhile, from the Fig. 9 is following that the potential of the output MCP electrode has not practically affected on the photoelectron stream trajectory. However, it is of great importance in multiplying the electron stream.

Important to select the optimal angle of deviation of the MCP channel's axis relative to the normal vector to

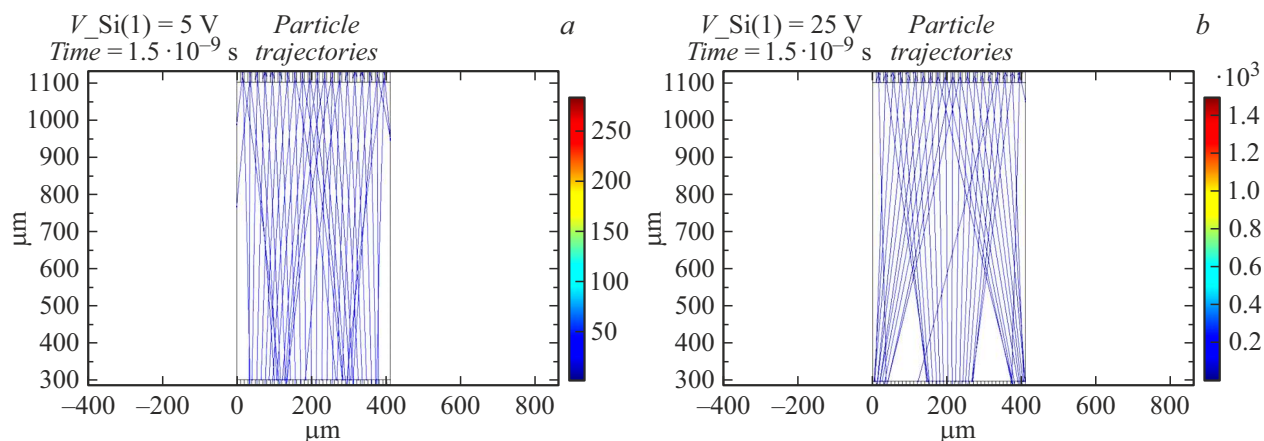


**Figure 5.** The electron trajectory between the silicon membrane and the MCP at potentials 5 (a) and 25 V (b) on the membrane.

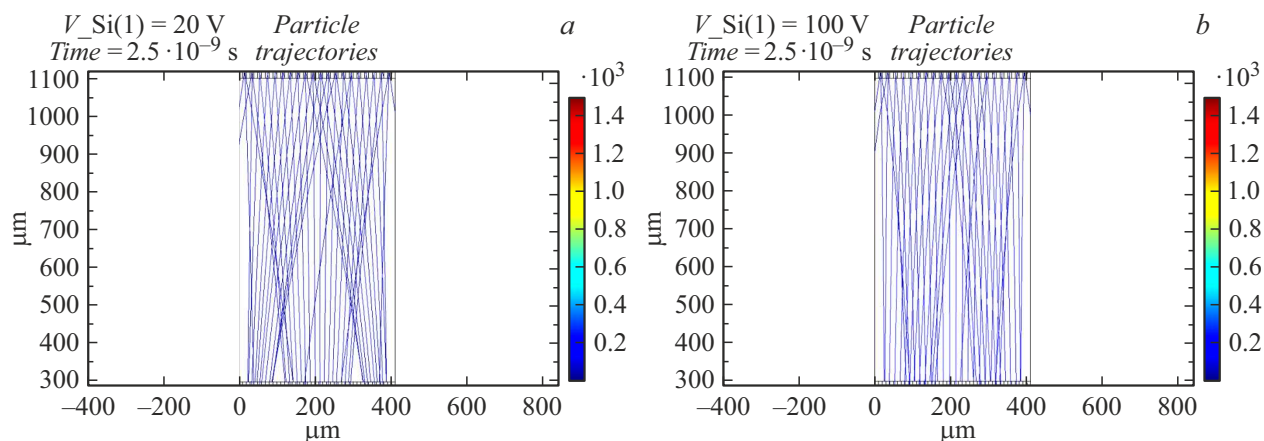


**Figure 6.** The electron trajectory in the space between the silicon membrane and the MCP at potentials 20 (a) and 100 V (b) at the top electrode of the MCP.

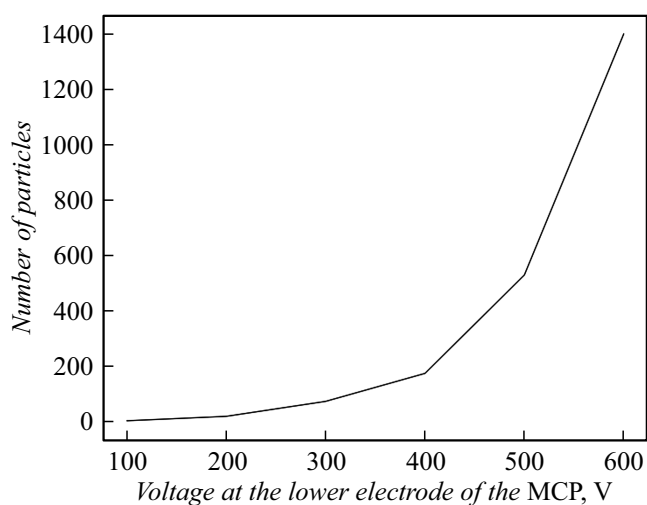


**Figure 7.** Dependence of the number of multiplied electron stream on the potential at the output electrode of the MCP at a fixed potential at the input electrode.

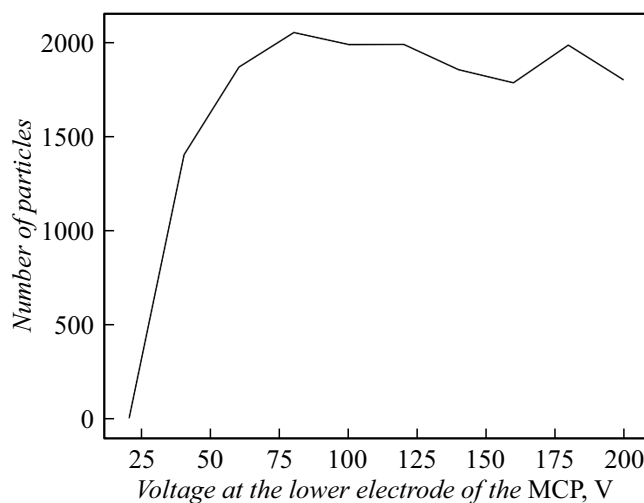


**Figure 8.** Dependence of the multiplied factor of the electron stream in the MCP on the value of the potential at the input electrode of the MCP (for a fixed potential difference of the MCP of 500 V).

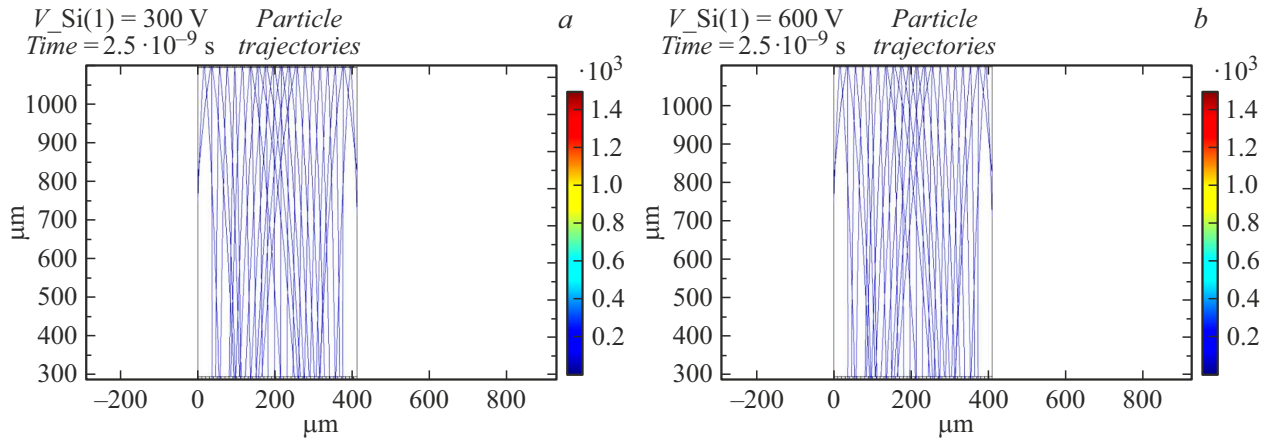


**Figure 9.** Electron trajectory between the silicon membrane and the input electrode of MCP at potentials at the input electrode of MCP at 300 V (a) and 600 V (b).

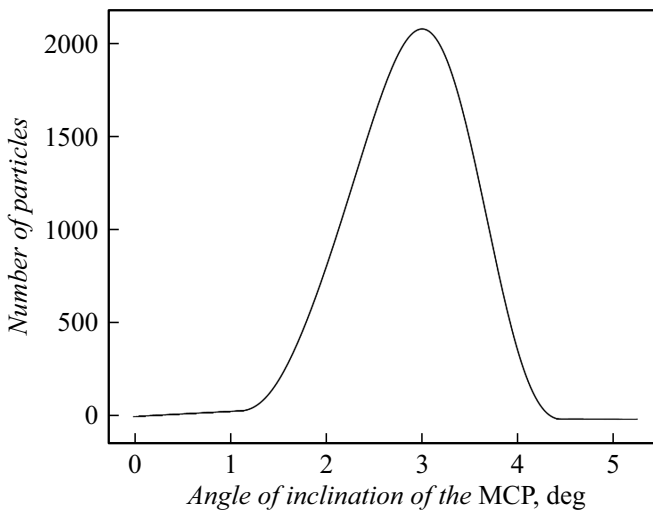


**Figure 10.** Dependence of the electron stream multiplication factor on the angle of orientation of the MCP channels relative to the optical axis of the product.

top MCP surface, which related to the maximum value of electron stream multiplication in the MCP. With an adjustment in the mentioned deflection angle, both the number of secondary electrons and the energy electrons will change for each cycle of multiplications. The calculations were carried out using the COMSOL Multiphysics software package, and the results are presented in Fig. 10.

From Fig. 10 it follows that the optimum angle of orientation of the MCP channel axes at a pair of formation energy of 10 eV, will be an equal  $\sim 3$  degrees. The calculations were carried out for the MCP thickness equal to  $150\ \mu\text{m}$ , and the value  $\sim 2000$  was obtained for the MCP multiplication factor:

$$G = \frac{n_{\text{output}}}{n_{\text{input}}}, \tag{12}$$

where  $n_{\text{input}}$  — is the number of electrons at the MCP input,  $n_{\text{output}}$  — is the number of electrons leaving the MCP.

Thus, the MCP multiplication factor can be represented by the expression (13):

$$G = n_{\text{secondary}}^{m_{\text{collision}}} \tag{13}$$

(where  $m_{\text{collision}}$  — is the number of cycles of secondary interactions of electrons with the surface of MCP channels), which means that a twofold increase in the MCP thickness leads to a quadratic change in the electron stream multiplication factor.

The optimum value of the potential of the input electrode MCP equals  $\sim 100\ \text{V}$  (Fig. 8), because it will provide the maximum multiplication factor of the MCP, and minimizes the defocusing of the electron stream. The results of calculations showed that the potential value of the output MCP electrode with a thickness of  $150\ \mu\text{m}$  should be  $\sim 500\text{--}600\ \text{V}$  in order to realize the electron stream multiplication factor by  $\sim 2000$  times at the pair formation energy  $\sim 10\ \text{eV}$ . The optimum orientation angle with the above parameters will be  $\sim 3$  degrees.

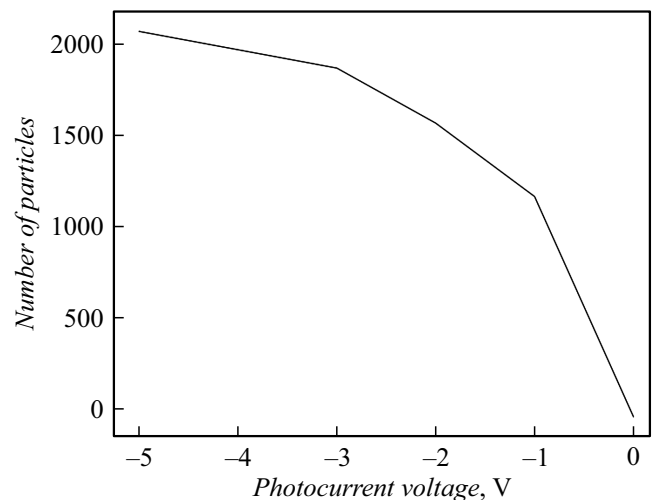


**Figure 11.** Impact of the photocathode potential on the captured photoelectrons number by the pyroelectric film.

**Table 1.** Basic parameters of control potentials and the angle of the MCP channels orientation of the thermal imager

Angle Orientation of MCP channels, deg	Potential of Silicon membranes, V	Potential of Photocathode, V	Potential of Top electrode MCP, V	Potential Lower electrode MCP, V	Potential of Electrode phosphor, V	Initial Energy of photoelectrons, eV
3	10	-1-0	100	600-1100	3000	0.5-1

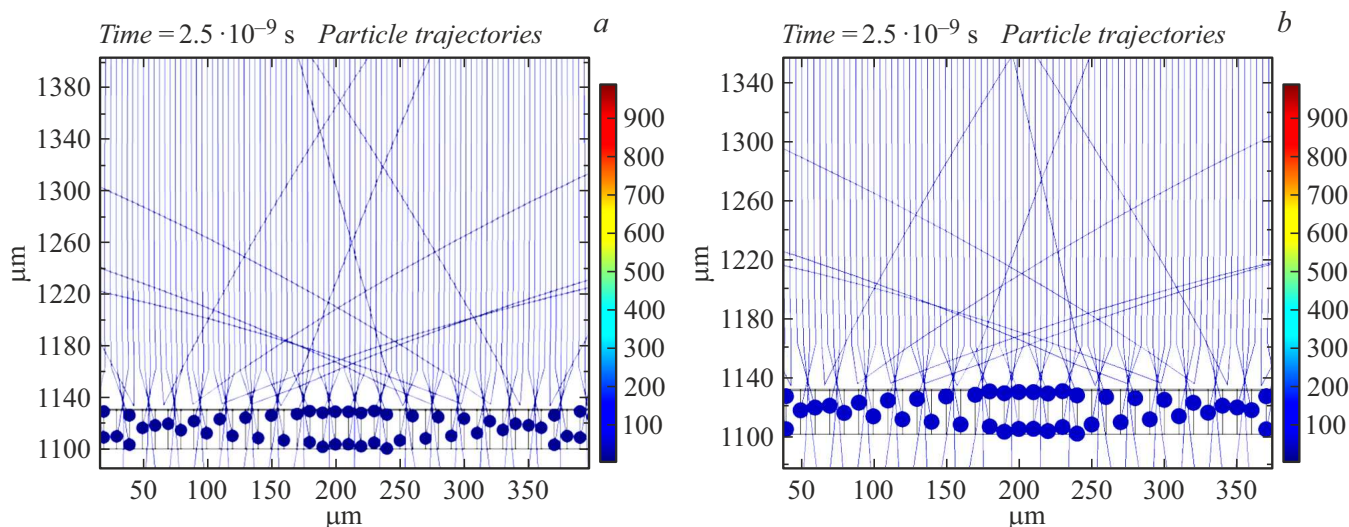


**Figure 12.** Photoelectron trajectories between a photocathode and a silicon membrane during local heating in the central area (a) and the right sector (b) of the pyroelectric film surface in the presence of a spontaneous polarization potential.

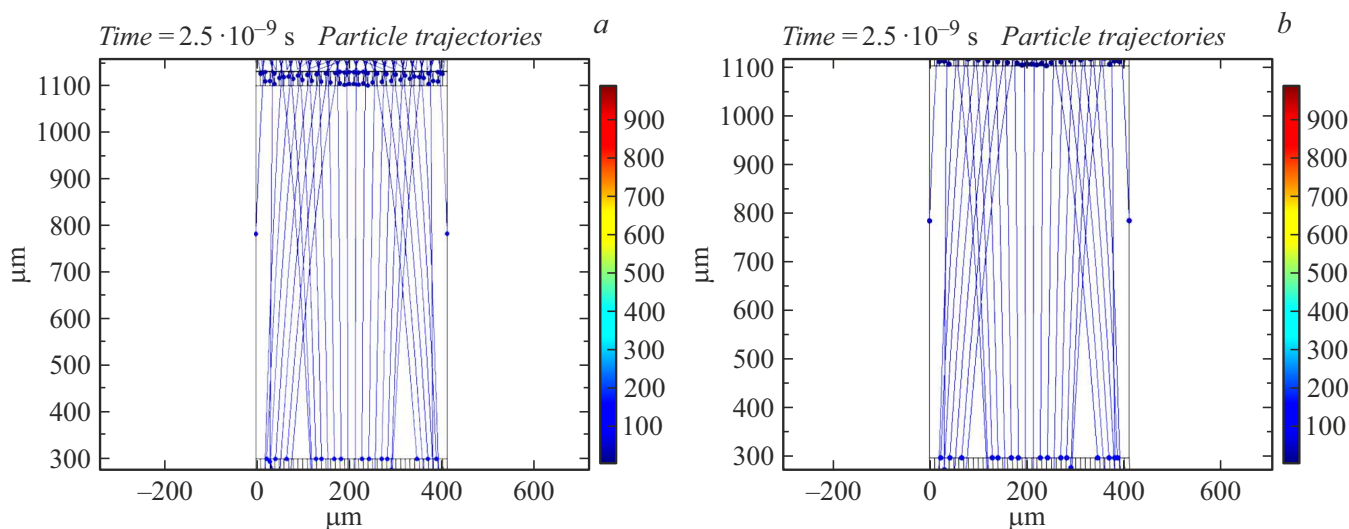


**Figure 13.** Photoelectron trajectories between a silicon membrane and MCP during local heating in the central area (a) and the right sector (b) of the pyroelectric film surface in the presence of a spontaneous polarization potential.

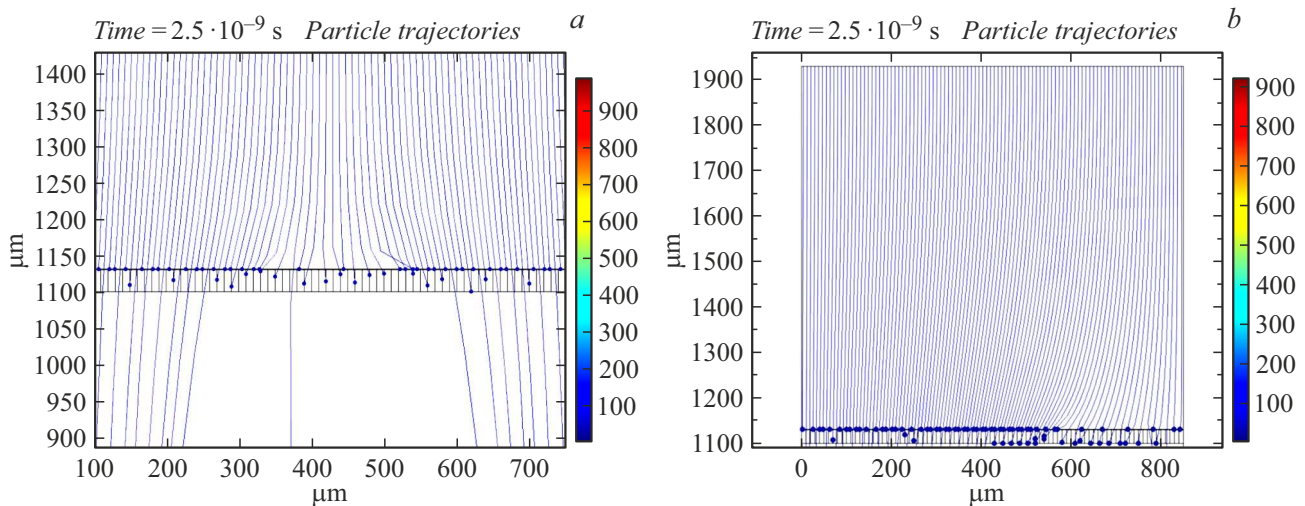


**Figure 14.** Photoelectron trajectories of the readout beam between a photocathode and a silicon membrane during local heating in the central area (a) and the right sector (b) of the pyroelectric film surface in the absence of a spontaneous polarization potential.

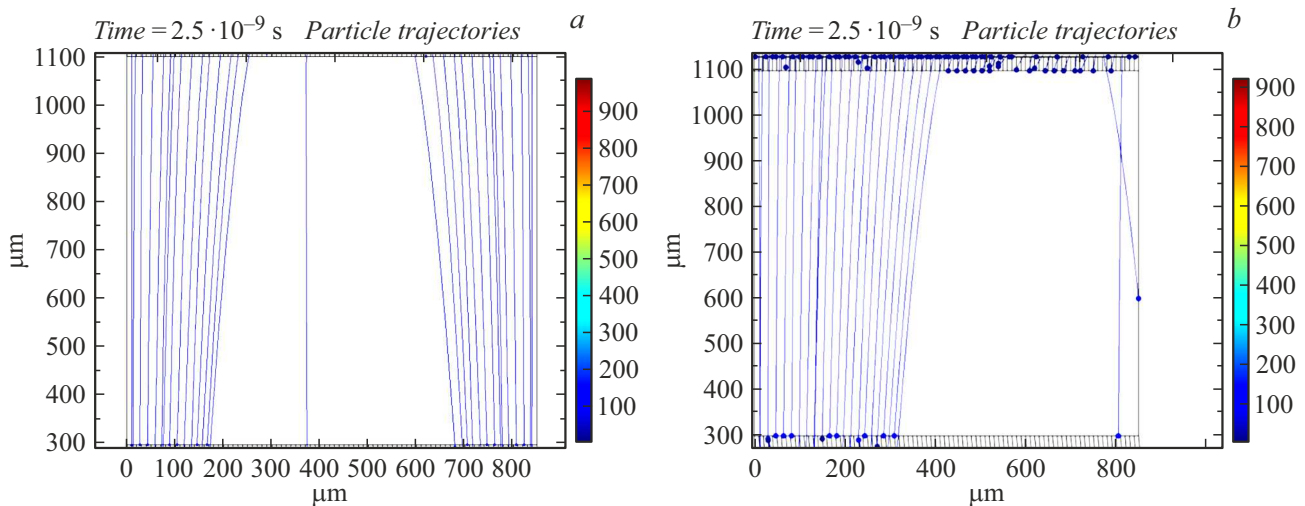


**Figure 15.** Photoelectron trajectories between a silicon membrane and MCP during local heating in the central area (a) and the right sector (b) of the pyroelectric film surface in the absence of a spontaneous polarization potential.

### 1.3. Investigations and search of photocathode potential

When searching the photocathode control potential value, it is required to ensure close values of the photoelectron energies and the energies of pyroelectric potentials. In the Figure 11 it presented the dependence of the photoelectrons captured number by the pyroelectric film on the photocathode potential at the potential at the input electrode of the MCP  $\sim 100$  V and the potential of the silicon membrane  $\sim 10$  V.

The functional dependence presented above allows to choose the optimum value of the photocathode potential, which is in the range  $(-1.0) - (-0.5)$  V.

Thus, as a result of calculations, the optimum values of the potentials and the optimal angle of the inclination axis of the MCP channels, which are presented in the table.

## 2. Investigation of the effect of spontaneous polarization of a pyroelectric film on the sensitivity of a thermal imager

### 2.1. The investigation of pyroelectric potential in the case of taking into account the influence of spontaneous polarization

The effect of spontaneous polarization of a pyroelectric film on sensitivity of the thermal imager was studied. This was carried out via model of reading node of a thermal imager, which is calculated the electron readout stream trajectory in the case of a nonuniform heating of pyroelectric film.

In particular, the case of heating of the middle and edge (right) sectors of the pyroelectric film surface was reviewed.



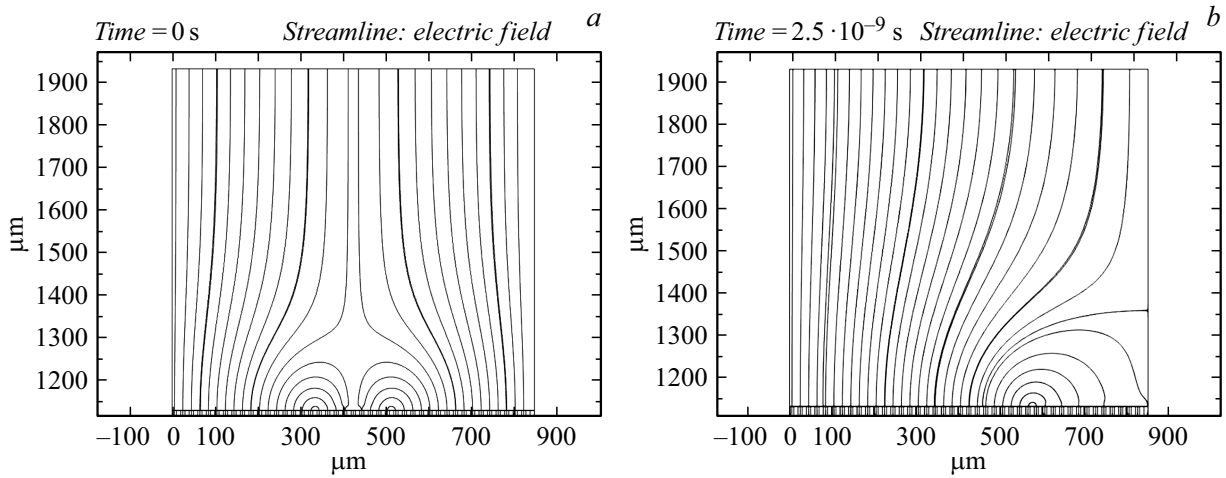


**Figure 16.** Electric field lines near the silicon membrane surface during local heating in the central area (a) and the right sector (b) of the pyroelectric film surface in the absence of a spontaneous polarization potential.

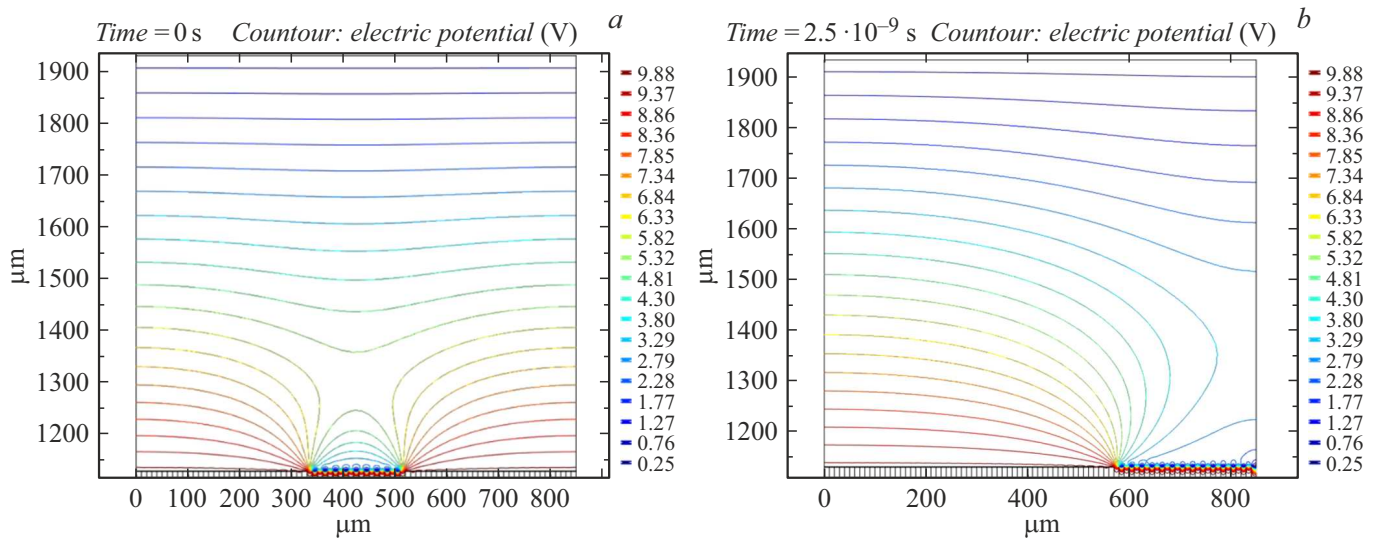


**Figure 17.** Equipotential lines near the silicon membrane surface during local heating in the central area (a) and the right sector (b) of the pyroelectric film surface in the absence of a spontaneous polarization potential.

A preliminary analysis [5] allowed to determine the range of the potentials induced by the thermal field. It amounted to  $\sim 1\text{--}2\ \mu\text{V}$  at a distance to the thermal object  $\sim 100\ \text{m}$  (thermal radiation power  $\sim 0.2\ \mu\text{W}/\text{cm}^2$  and  $10\text{--}15\ \mu\text{V}$  for the distance to the thermal object  $\sim 30\ \text{m}$ ). From the results presented in refer [5], the value of induced by heating surface potential  $\sim 1\ \mu\text{V}$  and the value of the surface potential of spontaneous polarization (i.e., in the cold area of the film)  $-1\ \text{V}$  was used.

To assess the opportunity of reading information from the surface induced potentials in the presence of a spontaneous polarization potential, between the photocathode and the silicon membrane (Fig. 12) and between silicon membrane and the MCP (Fig. 13) photoelectron stream trajectories were plotted.

From figures 12 and 13 are followed that the getting figures of the reading electron streams trajectories are no different to each other, thus for getting the information about a thermal object and the surrounding area the reset or compensation of the spontaneous polarization potential is required.

## 2.2. The investigation of pyroelectric potential in the case a preliminary reset or compensation of spontaneous polarization

In case of reset or compensation of the spontaneous potential, the opportunity of reading the information about a thermal object and the surrounding area is implemented, that it can see from Figs 14 and 15 where are demonstrated

the electron streams trajectories they pass through sections of inhomogeneously heated areas of the pyroelectric film.

The nature of the electron stream trajectory corresponds to the electric fields space distribution between the photocathode and the silicon membrane (Figs 16 and 17).

Thus, in case of reset of the spontaneous polarization potential of the pyroelectric film, the dual-spectral single-channel emission thermal imager of the IIT architecture can be used to reading images and the surrounding area.

## Conclusion

A physical and mathematical model has been formulated that allows to study the processes occurring in the basic units of a single-channel dual-spectral thermal imager, made in the IIT architecture. Using the COMSOL Multiphysics software package, the optimum values of control potentials and designs of the basic units of the thermal imager were determined, which provide the opportunity of reading and recognizing images of thermal objects and the surrounding area. The necessity of necessary reset (or compensation) of the spontaneous polarization potential is presented. The results of the study will be useful in the development of an innovative uncooled single-channel dual-spectral thermal imager, implemented in the IIT architecture.

## Funding

This research was supported financially by the Russian Foundation for Basic Research (project No. 20-38-90125).

## Conflict of interest

The authors declare that they have no conflict of interest.

## References

- [1] U. Adomeit. *SENSOR+TEST Conf. 2009* (Nürnberg, AMA Service GmbH, 2009), p. 221–226.  
DOI: 10.5162/irs09/i2.3
- [2] O. Cocle, C. Rannou, B. Forestier, P. Jouglu, P.F. Bois, E.M. Costard, A. Manissadjian, D. Gohier. *Infrared Technology and Applications XXXIII*, ed. by B.F. Andresen, G.F. Fulop, P.R. Norton (Proc. Orlando, SPIE, 2007), p. 654234, v. 6542.  
DOI: 10.1117/12.723720
- [3] H. Vogel, H. Schlemmer. *Detectors and Associated Signal Processing II*. Ed. by J.-P. Chatard, P.N.J. Dennis (Proc. SPIE, Jena, 2005), p. 59640S, v. 5964.  
DOI: 10.1117/12.625180
- [4] L. Feldman, D. Mayer. *Fundamentals of surface analysis and thin films* (Mir, M., 1989), p. 49.
- [5] A.S. Grevcev, P.A. Zolotukhin, E.A. Ilyichev, G.N. Petrukhin, A.V. Popov, G.S. Rychkov. *ZhTF*, **92** (4), 507 (2022).  
DOI: 10.21883/JTF.2022.04.52237.270-21